Journal of Materials Chemistry C

RSC Publishing

PAPER

View Article Online
View Journal | View Issue

Cite this: J. Mater. Chem. C, 2013, 1, 7400

Impact of 2,6-connectivity in azulene: optical properties and stimuli responsive behavior†

Michael Koch, Olivier Blacque and Koushik Venkatesan*

Received 15th August 2013
Accepted 16th September 2013

DOI: 10.1039/c3tc31610f

www.rsc.org/MaterialsC

The possible incorporation of the redox active, small donor acceptor molecule azulene as a core structure for potential optoelectronic applications has been evaluated. The synthesis and characterization of different isomers of di(phenylethynyl)azulene **1–4** have been successfully carried out. The photophysical properties as well as their stimuli responsive behavior reflecting their corresponding electronic properties were also investigated. The experimental observations show that 2,6-connection (**3**) exhibits intense luminescence and shows the strongest stimuli responsive behavior upon acid treatment. DFT calculations of **3** reveal the highest contributions of the alkyne substituents at the 2- and 6-position of the azulene to the ground- and excited state that makes the 2,6-connectivity at azulene a very promising candidate for low band-gap conjugated materials.

Introduction

Design and synthesis of novel conjugated polymers have been intensely investigated over the last two decades due to their extensive application as optoelectronic materials.[1–9] In particular, conjugated polymers have been utilized in a wide variety of transduction schemes to realize sensitive and highly selective detection of chemical and biological analytes by taking advantage of their stimuli responsive behavior.[10–17] Due to azulene's unique electronic and optical properties such as large permanent dipole moment, intense blue color and the domination of fluorescence from $S_2 \rightarrow S_0$ with low emission intensity, due to the violation of Kasha's rule,[18–20] it has been long considered to be an interesting candidate for application in optoelectronic materials (see Fig. 1).[21,22]

However, the evaluation of azulene as a core structure for optoelectronic applications remains scarce, although calculated theoretical results using various aromaticity theories suggest that azulene possesses a much lower delocalization energy (4.2 kcal mol^{-1}) in comparison with benzene (20 kcal mol^{-1}), thiophene (16.1 kcal mol^{-1}) and naphthalene (30.5 kcal mol^{-1}).[23] Recently Hawker's group and our group reported on the stimuli responsive behavior of azulene derivatives. The treatment of azulene derivatives with superacids results in an azulenium cation upon protonation at the unsubstituted 1-position with the concomitant increase in luminescence intensity. This is accompanied by a bathochromic shift of the emission wavelength especially in the case of ethynyl spacer bearing groups. The $S_1 \rightarrow S_0$ transition becomes the dominant radiative decay pathway of the protonated species.[24–26] Such a response of azulene towards superacids not only allows one to control the emission properties, but also permits to tailor the conducting properties of the azulene as recently demonstrated by Hawker and co-workers.[27]

Despite quite a large number of theoretical calculations on the influence of the functional bis-substitution pattern of azulenes on their electronic properties, the experimental investigations have been rather limited.[28,29] Based on theoretical calculations, the 2,6-connected polyazulenes are expected to be most unique compared with other substitution patterns. The π-electrons can easily delocalize along the direction of the dipolar C_{2v} axis of azulene resulting in a large dipole moment and large hyperpolarizability. This is especially supported by the ability to form an expected quinoid structure. 2,6-connected azulene systems would thus possess a lower band gap than the otherwise connected azulene polymers, which is also highly interesting for preparing low band-gap conducting

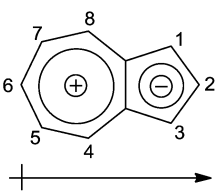

Fig. 1 Mesomeric structure of azulene with the numbering scheme and permanent dipole moment.

Institute of Inorganic Chemistry, University of Zurich, Winterthurerstrasse 190, CH-8057 Zurich, Switzerland. E-mail: venkatesan.koushik@aci.uzh.ch; Fax: +41 44-635-68-03; Tel: +41 44-635-46-94

† Electronic supplementary information (ESI) available: Contains experimental details, characterization data and various NMR spectra. Additional figures showing molecular orbitals, calculated spectra and Cartesian coordinates are also provided. See DOI: 10.1039/c3tc31610f

polymers for application in organic solar cells.[29,30] In these polymers, the highest symmetry of C_{2v} will be preserved in the planar form, while in all the other possible polymers of azulene a much lower symmetry is expected because in the latter cases the monomer symmetry axis does not equal the polymeric symmetry axis. Also, the polymer consisting of only a 2,6-connectivity will show a head-to-tail alignment of the monomeric dipole moments.

While there are many examples of mono-alkyne substituted azulenes reported in the literature, dialkyne substituted azulenes remain scarce except for the ones exclusively bearing the alkynes at the 1- and 3-position of the azulene.[26,31–38] The only known 2,6-bissubstituted compounds either bear an alkyne or an alkyl chain at the 6 position, or they are connected to a metal center as a bridging ligand or, are part of a 6,6'-connected azulene dimer.[39–42]

In this work, we report the systematic synthesis of 2,6-diphenyl acetylene substituted azulene and investigation of its stimuli responsive behavior as a model compound for macromolecules. Di(phenylethynyl) substitution was particularly chosen in order to allow for easy correlation of the properties as model compounds. For comparison reasons, we have also prepared the three other isomers of di(phenylethynyl)azulenes **1**, **2** and **4** (see Fig. 2).[43]

Synthesis of specific substitution patterns on azulene is quite challenging and difficult to achieve,[44,45] and since there is no common starting material available to prepare the target molecules, different approaches had to be sought to accomplish the desired molecules (see Scheme 1). Given the unique interesting properties expected to arise from the 2,6-connectivity in azulene, we set out to develop a synthetic strategy that would not only allow one to achieve the targeted 2,6-diphenyl substituted azulene, but would also offer considerable modularity in synthesis, starting from 2-bromo-6-phenylethynyl azulene (**14**). To the best of our knowledge, this work represents the first such experimental study combined with a deeper theoretical insight provided by DFT calculations into the optoelectronic behavior of an azulene core including the targeted synthesis and photophysical evaluation of the elusive 2,6-alkyne substituted azulene **3**.

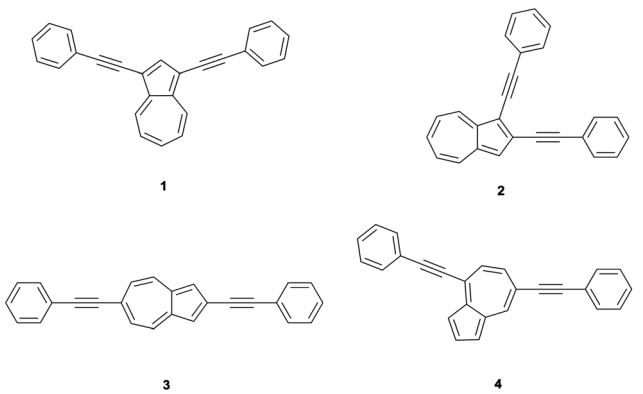

Fig. 2 Structures of di(phenylethynyl)azulenes **1**, **2**, **3** and **4**.

Synthesis

Since the synthesis of **1** has been already known in the literature,[32] our detailed discussion pertains only to the synthesis and properties of the new compounds **2**, **3** and **4**. As previously mentioned, we utilize different approaches as shown in Scheme 1.[46] **1** was synthesized starting from the dark green colored 1,3-diiodoazulene **6**, which in turn was prepared in excellent yields (98%) by reacting the commercially available compound **5** with 2 eq. *N*-iodosuccinimide (NIS) in dry CH_2Cl_2. Subsequent application of Sonogashira coupling conditions consisting of an excess amount of phenyl acetylene and catalytic amounts of CuI, PPh_3 and $Pd(PPh_3)_2Cl_2$ in the presence of an excess amount of Et_3N at elevated temperature gave **1** as a blue green colored solid in very good yield (91%).

Compound **2** was prepared from the known 2-phenylethynylazulene **7**.[26] The mono-alkyne **7** was treated with 1 eq. NIS in dry toluene below 10 °C to minimize diiodination, to give green 1-iodo-2-phenylethynylazulene **8** which decomposes in solid state and is stable in solution only for a couple of days. Therefore the filtered reaction mixture was directly utilized in the Sonogashira coupling reaction leading to green **2** in a good overall yield (91%).

Despite the synthesis of **3** involving many steps due to the challenging substitution pattern, we were able to obtain the targeted compound in an overall yield of 21%. A direct synthesis of the 2,6-pattern is not feasible since it requires an electrophilic attack at the electron rich five membered ring for the substitution of the 2-position which is more favored at the more nucleophilic 1- and 3-positions, while on the other hand a mandatory nucleophilic attack at the electron poor seven membered ring will be directed to the 4- and 8-position and not result in the desired 6-substitution. Therefore the parent azulene **5** cannot be directly used as a precursor for the synthesis of 2,6-dialkyne azulene, but instead starting material (**9**), based on the work of Nozoe and co-workers and the work of Ito and co-workers,[39,47,48] was utilized in which the 1- and 3-positions bearing ethyl ester protected groups shielded the 4- and 8-position from a nucleophilic attack.

Starting from the orange colored diethyl 2-hydroxyazulene-1,3-dicarboxylate **9**[49] the hydroxyl-group was alkylated with methyl iodide to give the known bright red product **10** in very good yields (91%). This product was brominated at the 6-position to result in the known orange product **11** in 85% yield. The ester-functionalities act as protection groups in this step. Due to sterical hindrance, the nucleophilic bromination at 4- and 8-positions is blocked resulting in an exclusive bromination at the 6-position. Sonogashira coupling with phenyl acetylene gave the mono-alkyne product **12** in 83% yield, which was subsequently thermally dealkoxycarboxylated to give 2-hydroxy-6-phenylethynyl-azulene **13** in 56% yield. Conversion of the hydroxyl-group with PBr_3 to **14** (68%) followed by Sonogashira coupling gave eventually **3** as a dark green product in 96% yield.

4 was synthesized as a blue colored product in very good yields (93%) starting from the known 4,7-dibromoazulene **15** under Sonogashira conditions.[25]

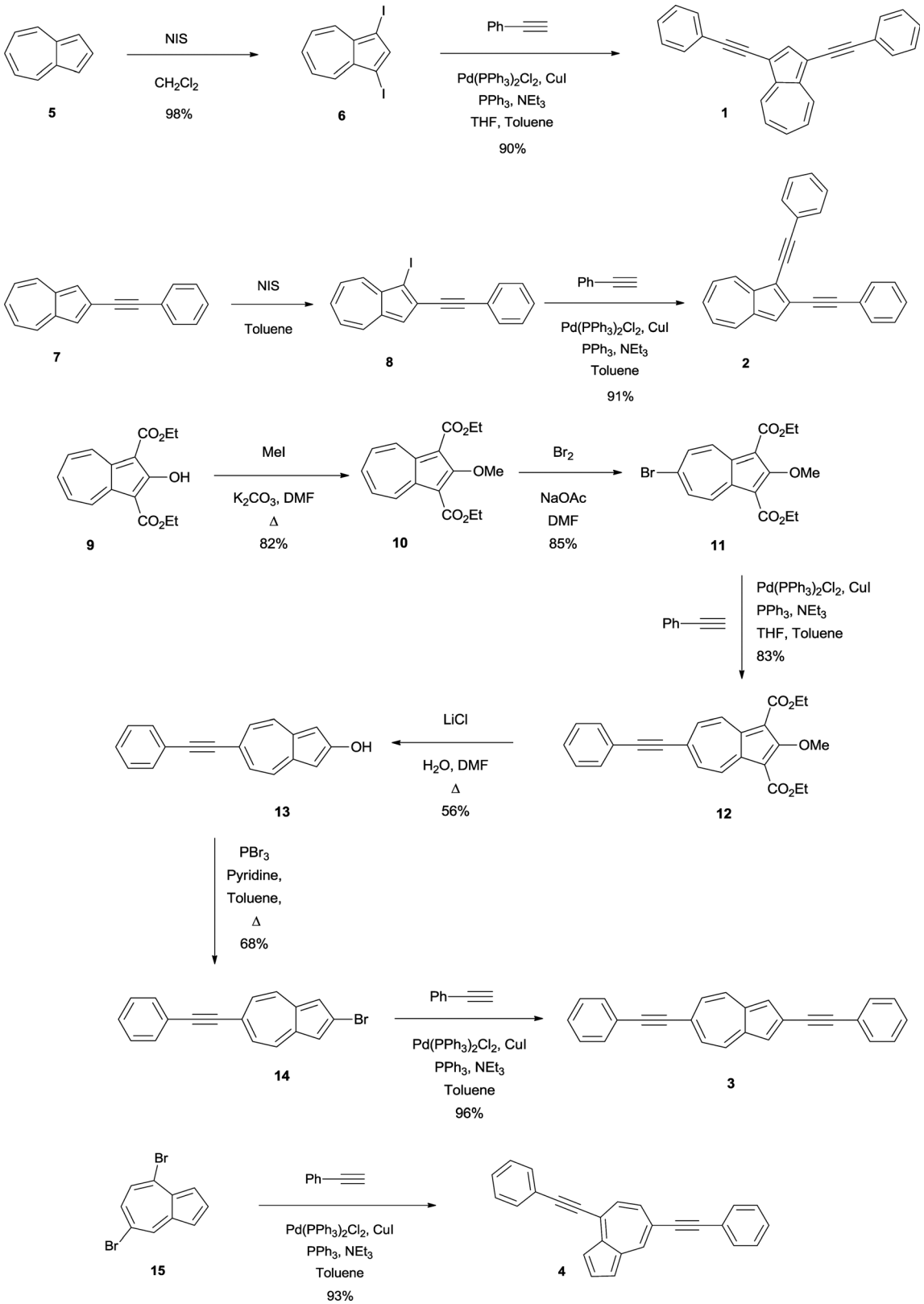

Scheme 1 Synthesis of di(phenylethynyl)azulenes **1**, **2**, **3** and **4**.

UV-Vis studies

The UV-Vis absorption spectra of **1–4** can be classified into three regions: the first region for $\lambda > 500$ nm which is composed of the $S_0 \rightarrow S_1$ transitions, the second region for 370 nm $< \lambda <$ 500 nm showing the $S_0 \rightarrow S_2$ transitions and the third region for $\lambda < 370$ nm comprising the $S_0 \rightarrow S_3$ transitions.

The UV-Vis absorption spectra of **1–4** exhibit high molar extinction coefficients in the region $\lambda < 500$ nm (see Fig. 3). In the region of $\lambda > 500$ nm compound **4** possesses the most broad absorption band between 520 nm and 800 nm among the synthesized compounds; however the intensity of the band was low and similar to that found for the parent azulene (**5**). A similar band could only be detected at much higher concentrations in the spectra of **1**, **2** and to an even lesser extent for **3**. This difference can be ascribed to the fact that the desired electronic contribution of the substituents to the transition is less pronounced for **4** while it is strongest for **3** (see also DFT calculations). In the region that is assigned to the $S_0 \rightarrow S_2$ transition (*ca.* 370–500 nm) **1** and **2** reveal only a small molar extinction coefficient in comparison to **3** and **4**. It is evident from this observation that the position of the substitution alters the probability of the two possible transitions that govern azulene's absorption behavior. This is especially the case for **3** that shows similar intensities for both transitions. Additionally **3** shows the highest molar extinction coefficient in this red shifted region (44000 M^{-1} cm^{-1} compared to 10400 M^{-1} cm^{-1} (**1**), 14000 M^{-1} cm^{-1} (**2**), 34000 M^{-1} cm^{-1} (**4**)). Since azulene's fluorescence results from excited state S_2, a transition in this wavelength region with a high molar absorption coefficient is crucial (see Table 1). Furthermore tuning of this band to longer wavelength is desired due to the fact that this correlates with a smaller energy gap of the transition and better polarizability of the molecule. In the region assigned to the $S_0 \rightarrow S_3$ transition ($\lambda < 370$ nm), the extinction coefficients as well as the absorption wavelength vary only to a certain extent.

Azulene's optical behavior is tremendously changed upon protonation (see Fig. 4 and 5), since the emission of the protonated species results from the S_1 states. The corresponding $S_0 \rightarrow S_1$ transition is observed in the UV-Vis absorption spectra in the region of *ca.* 420–580 nm for **1-H$^+$**–**4-H$^+$**. After protonation, significant changes in the UV-Vis absorption spectra were observed.[50]

4-H$^+$ showed a very distinct absorption band centered around 490 nm with a high molar extinction coefficient ($\varepsilon = 57800$ M^{-1} cm^{-1}, see Fig. 6). **3-H$^+$** exhibited an even more distinct absorption band combined with the highest molar extinction coefficient in comparison with the rest of the protonated isomers (525 nm, $\varepsilon = 77100$ M^{-1} cm^{-1}) and in fact even higher than the extinction coefficients of the untreated isomers **1–4**. Although compounds **1-H$^+$** and **2-H$^+$** also display an absorption band in this region, they are not distinct and have significantly lower intensities, especially in the case of **1-H$^+$**. **1-H$^+$** and **2-H$^+$** display after protonation an additional broad but low intensity band with a bathochromic shift at 703 nm (**1-H$^+$**) and 689 nm (**2-H$^+$**) respectively (see Fig. 6), which is neither

Table 1 Absorption and emission data (nm) of unprotonated and protonated species in CH_2Cl_2 at rt

	Unprotonated		Protonated[a]	
Compd.	λ_{max} (abs)	λ_{max} (em)	λ_{max} (abs)	λ_{max} (em)
5[b]	340	376	355	422
7[b]	401	424	471	533
1	423	465	703	722[c]
2	418[d]	432	689[e]	733
3	446	484	525	571
4	409	416	490	537

[a] Treated with $MeSO_3H$ [b] Literature values.[26] [c] Extremely weak emission. [d] Shoulder. [e] Very broad band with low intensity.

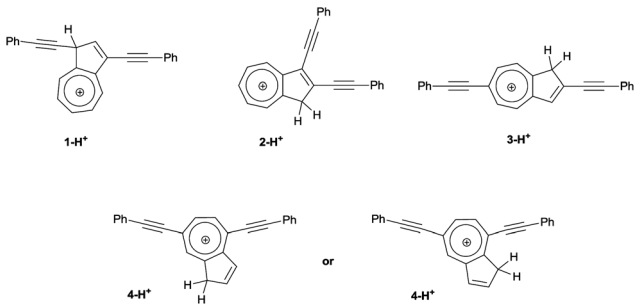

Fig. 4 Plausible structures of di(phenylethynyl)-azulenes after treatment with superacids.

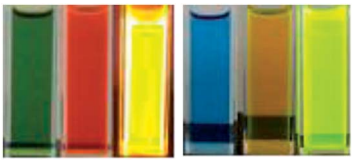

Fig. 5 *Left*: Photo of **3** (CH_2Cl_2, treated with $MeSO_3H$, treated with $MeSO_3H$ (exc. at 365 nm)). *Right*: Photo of **4** (CH_2Cl_2, treated with $MeSO_3H$, treated with $MeSO_3H$ (exc. at 365 nm)).

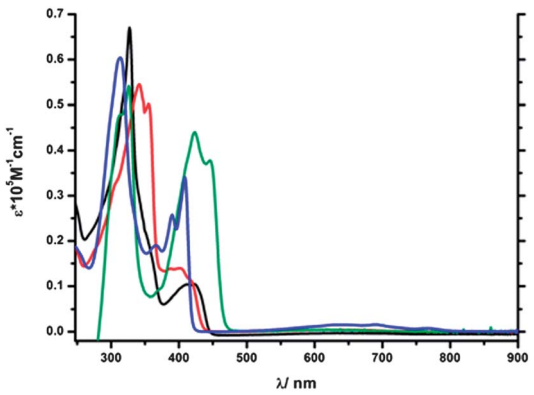

Fig. 3 UV-Vis absorption spectra of **1** (black line), **2** (red line), **3** (green line) and **4** (blue line) in CH_2Cl_2.

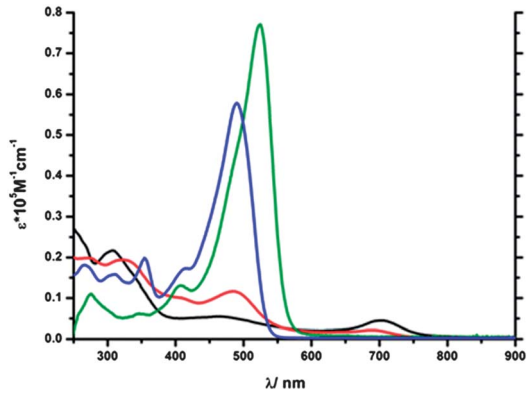

Fig. 6 UV-Vis absorption spectra of **1-H⁺** (black line), **2-H⁺** (red line), **3-H⁺** (green line) and **4-H⁺** (blue line) in CH_2Cl_2.

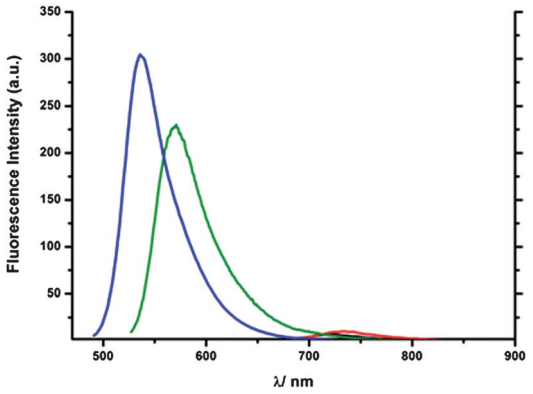

Fig. 8 UV-Vis emission spectra of **1-H⁺** (black line), **2-H⁺** (red line), **3-H⁺** (green line) and **4-H⁺** (blue line) in CH_2Cl_2.[50]

observed in the **3-H⁺** and **4-H⁺** nor in the protonated 2-phenylethynylazulene (**7**).

The emission spectra reveal the intensity of **1** to be very weak, while **2** is only slightly stronger; **3** and **4** show a substantial fluorescence intensity although much stronger in the case of **4** but more red shifted in the former case (see Fig. 7). The low emission intensity of **1** and **2** can be caused by the transfer of the additional electron density into the five membered ring and the limited contribution of the phenylethynyl substituents to states relevant for the transition. The emission bands were found to be located in the range of *ca.* 70 nm (416 nm to 484 nm). In this context **3** showed the most red shifted emission band among all the isomers although it is not as intense as that of **4** but is the most broad band (*ca.* from 430 nm to 650 nm). **4** shows a more significant hypsochromic shift in the emission wavelength than the mono-alkyne compound 2-phenylethynylazulene **7** (424 nm). Upon protonation the emission intensity of azulene compounds was expected to increase substantially as it was shown for other related compounds.[25,26] Nevertheless in the case of **2-H⁺**, only a slightly more intense emission was observed (see Fig. 8) and in the case of **1-H⁺**, the emission was even barely detectable revealing that both connection patterns are not promising candidates for stimuli responsive materials. The emission wavelengths of **2-H⁺** (733 nm) and **1-H⁺** (722 nm) are strongly red-shifted. This can be explained based on the dipole-moment of the excited state of the protonated compounds, which is diametrically opposed to the ground-state dipole-moment, and therefore points in the direction of the seven-membered ring. **3-H⁺** and to a lesser extent **4-H⁺** display strongly increased emission intensity making both connection patterns promising candidates for stimuli responsive materials. Nevertheless the fluorescence wavelengths were found to be less red shifted than in the case of **1-H⁺** and **2-H⁺**. In this context **3-H⁺** is more bathochromically shifted than **4-H⁺** and exhibits a significantly stronger stimuli response than all other isomers. The smaller shift can be explained by the fact that the distance of the charge-transfer is longer in **1-H⁺** and **2-H⁺**.

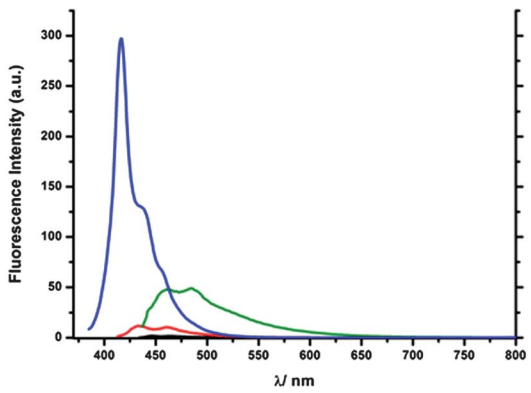

Fig. 7 UV-Vis emission spectra of **1** (black line), **2** (red line), **3** (green line) and 4 (blue line) in CH_2Cl_2.[51]

DFT calculations

All calculations were performed with the Gaussian 09 program package[52] using the hybrid functional PBE1PBE[53] in conjunction with the cc-pVDZ basis set.[54] Full geometry optimizations without symmetry constraints were carried out in the gas phase for the singlet ground states (S_0). The optimized geometries were confirmed to be potential energy minima by vibrational frequency calculations at the same level of theory, as no imaginary frequency was found. The first twenty singlet–singlet transition energies were computed at the optimized S_0 geometries by using the time-dependent DFT (TD-DFT) methodology.[55–57] Solvent effects were taken into account using the conductor-like polarizable continuum model (CPCM)[58,59] with dichloromethane as solvent for the TD-DFT calculations on all optimized gas-phase geometries. The excited state structures were optimized by TD-DFT calculations, and the first four electronic transitions were computed taking into account the state-specific equilibrium solvation of each excited state at its equilibrium geometry.

The TD-DFT calculations performed at the PBE1PBE/cc-pVDZ level on the DFT optimized ground state geometries of the di(phenylethynyl)azulene compounds **1–4** (see Fig. S31–S35,

ESI†) confirm that the absorption spectra can be divided into three regions:

(1) $\lambda > 550$ nm: region with very weak absorption bands corresponding to the $S_0 \rightarrow S_1$ singlet–singlet transition. The S_1 excited states are derived from the HOMO → LUMO excitation for **1**, **2** and **4**, and from the HOMO−1 → LUMO excitation for **3**. The calculated oscillator strengths are very small in the range of 0.007–0.025, except for **4** which shows a significant value f of 0.159;

(2) $375 < \lambda < 550$ nm: region with moderate to intense absorption bands ($0.292 < f < 1.877$) corresponding to the $S_0 \rightarrow S_2$ singlet–singlet transition. The singlet S_2 excited states are derived from a combination of the HOMO → LUMO+1 and HOMO−1 → LUMO excitations for **1**, **2** and **4**, and from the HOMO → LUMO excitation for **3** which shows the highest oscillator strength for this transition;

(3) $300 < \lambda < 375$ nm: region with moderate to intense absorption bands ($0.137 < f < 1.805$) corresponding to the $S_0 \rightarrow S_3$ singlet–singlet transition. The S_3 excited state is derived from the HOMO → LUMO+2 excitation for **1**, the HOMO → LUMO+1 excitation for **2**, HOMO−2 → LUMO+2 for **3**, and mainly from the HOMO−1 → LUMO excitation for **4**.

The $S_0 \rightarrow S_1$ transitions are experimentally observed but appear as very weak and broad bands. The wavelength maxima of the $S_0 \rightarrow S_2$ transitions are quite similar for the di(phenylethynyl)azulene compounds except for **3** which shows a significantly red shifted band with the highest molar extinction coefficient. This observation holds well only in the case of **3** where the S_2 excited state arises directly from the HOMO and LUMO orbitals. In all cases, the occupied MOs involved in the $S_0 \rightarrow S_2$ transitions are of π character mainly located on the azulene core and to a lesser extent on one or both phenylethynyl substituents with a π bonding character of the C≡C triple bond(s) (see Fig. 9 and 10). Except for the LUMO of **2** which is only delocalized over the azulene moiety, LUMO and LUMO+1 show very similar compositions as HOMO−1 and HOMO, respectively, notably with an antibonding π^* character of the C≡C triple bond(s). The absorption data calculated for the protonated cationic species **1-H$^+$**–**4-H$^+$** are not as accurate as the values obtained for the neutral species (see Table 2). Indeed, the TD-PBE1PBE calculations failed to reproduce the additional broad bathochromic bands at 702 and 688 nm for **1-H$^+$** and **2-H$^+$**, respectively. Nevertheless, it appears that upon protonation the $S_0 \rightarrow S_1$ transition exhibits the largest oscillator strength of the first singlet–singlet transitions and corresponds to the HOMO → LUMO excitation (see Fig. 11).

Despite the mismatch of both the trends of the calculated absorption wavelengths, the $S_0 \rightarrow S_1$ oscillator strengths mimic well the relative molar extinction coefficients with $f = 0.019$ (**1-H$^+$**) < 0.612 (**2-H$^+$**) < 1.467 (**4-H$^+$**) < 2.069 (**3-H$^+$**). The main difference with the unprotonated species is that the LUMOs are of π/π^* character on the azulene rings but exhibit mainly nonbonding orbitals on the phenylethynyl substituents,

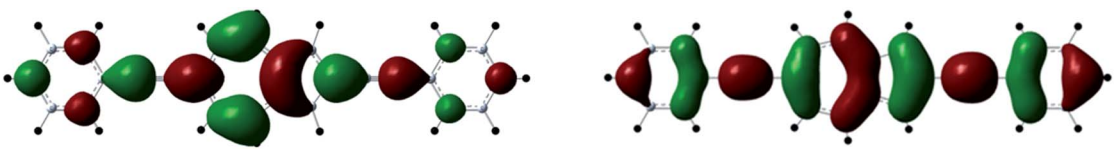

Fig. 9 Spatial plots of the HOMO (left) and LUMO (right) orbitals of the ground-state of **3**.

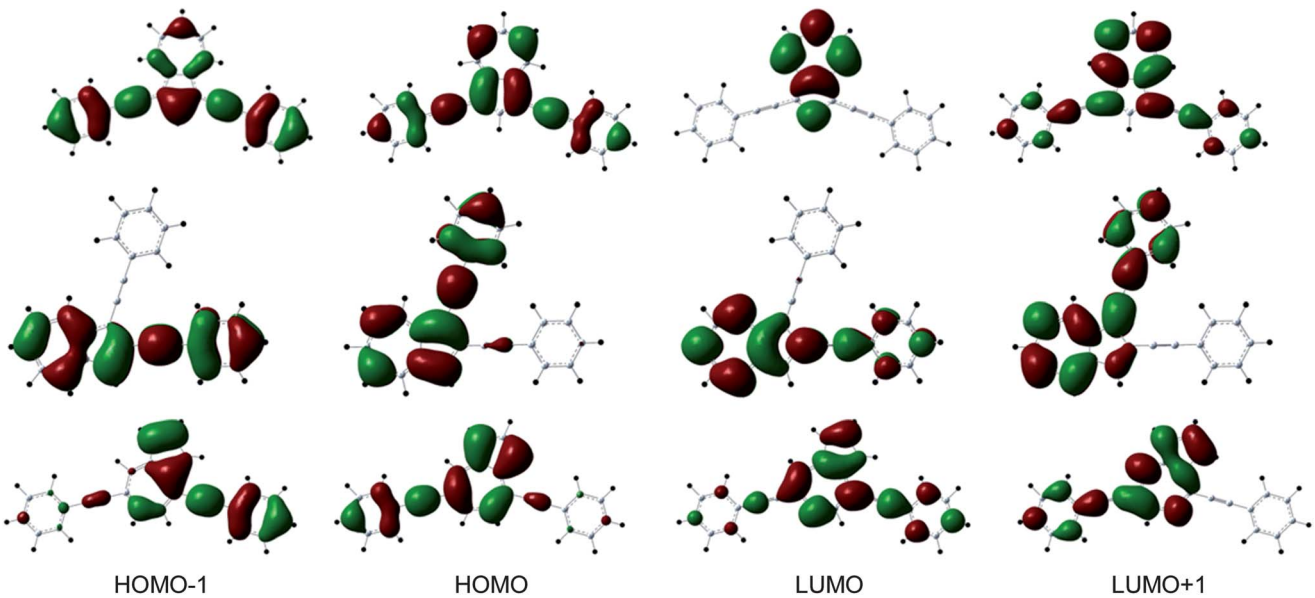

Fig. 10 Spatial plots of frontier orbitals of the ground-states of **1** (top), **2** (middle) and **4** (bottom).

Table 2 Selected singlet–singlet (S_0–Sn) transition energies (nm) and oscillator strengths *f* (in italics) for protonated **1-H$^+$–4-H$^+$** and unprotonated **1–4** species

	1	**2**	**3**	**4**	**1-H$^+$**	**2-H$^+$**	**3-H$^+$**	**4-H$^+$**
exp abs λ_{max}	423	418	446	409	703	689	525	490
exp em λ_{max}	465	432	484	416	722	733	571	537
TD-DFT on ground-state structures								
$S_0 \rightarrow S_1$	614.0	600.2	574.6	603.7	**492.6**	**536.7**	**518.4**	**505.6**
	0.007	*0.025*	*0.012*	*0.159*	*0.019*	0.612	*2.069*	*1.467*
$S_0 \rightarrow S_2$	**419.4**	**418.8**	**463.8**	**414.6**	475.0	494.3	456.6	448.5
	0.292	*0.331*	*1.877*	*0.972*	*0.026*	*0.039*	*0.022*	*0.170*
$S_0 \rightarrow S_3$	353.1	358.9	347.9	360.2	445.7	394.7	398.4	386.0
	1.345	*1.805*	*0.137*	*0.401*	*0.023*	*0.481*	*0.004*	*0.078*
TD-DFT on excited-state structures								
$S_1 \rightarrow S_0$					1317.5	**764.4**	**560.9**	**517.1**
					0.004	*0.131*	*1.006*	*1.257*
$S_2 \rightarrow S_0$	459.8	457.6	506.5	445.0	**754.6**	677.4	490.6	450.5
	0.222	*0.424*	*1.680*	*1.244*	*0.038*	*0.019*	*0.945*	*0.097*

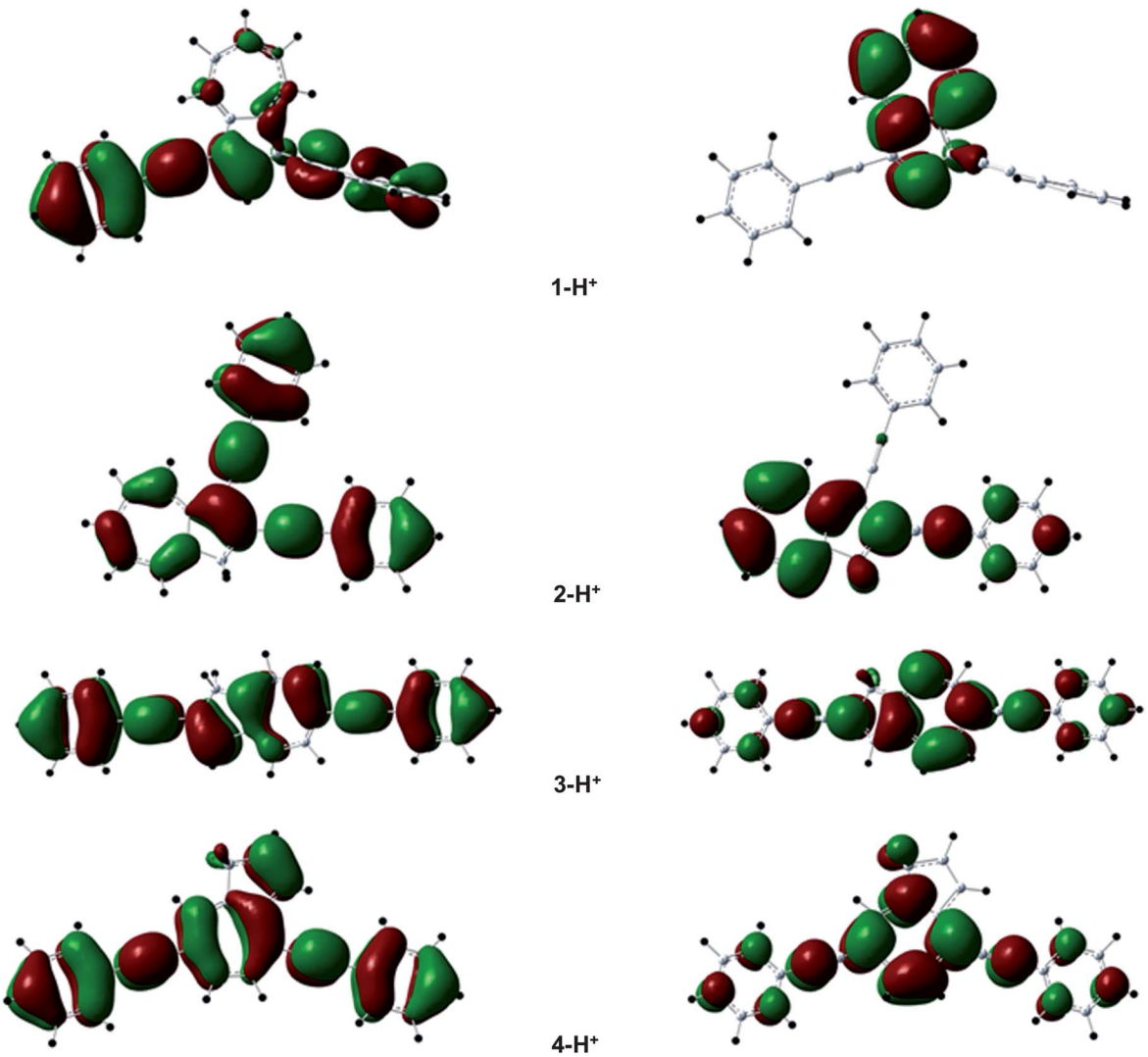

Fig. 11 Spatial plots of the HOMO (left) and LUMO (right) of the ground states of **1-H$^+$–4-H$^+$**.

suggesting a lesser participation of the latter in the absorption and fluorescence properties.

The first excited state (S_1) for the protonated species and the second excited state (S_2) for the neutral compounds were successfully optimized by TD-DFT at the same level of theory used for the DFT calculations (PBE1PBE/cc-pVDZ). Fluorescence wavelengths, energies and oscillator strengths were computed taking into account the state-specific equilibrium solvation of each excited state at its equilibrium geometry (see Table 2). The structural changes between the ground state and excited state structures are especially observed on the five-membered ring as well as on the alkyne substituents for the neutral compounds and, in contrast, only on the seven-membered ring for the protonated species (see ESI†, Fig. S21–S22). The $S_2 \rightarrow S_0$ fluorescence of **1–4** corresponds exactly to the $S_0 \rightarrow S_2$ absorption. The predicted wavelengths of the fluorescence maxima respectively of 460 (−5 nm compared to the exp. data of 465 nm), 458 (+26), 507 (+23), 445 (+29) nm are acceptable and interestingly the calculated oscillator strengths of 0.222, 0.424, 1.6803, and 1.244 reproduce well the relative fluorescence intensity of **1–4**, with **3** and **4** showing the most intense emission bands. For the protonated species, the same conclusion can be arrived at with the fluorescence maxima fitting correctly with the experimental data 755 (+33), 764 (+31), 561 (−10) and 517 (−20) for **1-H**$^+$ to **4-H**$^+$ respectively (except that in the case of **1-H**$^+$ it corresponds to the $S_2 \rightarrow S_0$ transition instead of $S_1 \rightarrow S_0$ for the other species) and also the oscillator strengths of 0.038 and 0.131 for **1-H**$^+$ and **2-H**$^+$, and of 1.006 and 1.257 for **3-H**$^+$ and **4-H**$^+$, corresponding well with the experimental features (see Fig. 8).

Conclusions

In summary, we have successfully synthesized four di(phenylethynyl)azulene isomers and experimentally demonstrated that 2,6-connection in azulene exhibits quite interesting and unique optical and physical properties in comparison with the other isomers of di(phenylethynyl)azulenes. UV-Vis absorption and luminescence properties were investigated to evaluate possible different incorporation positions of azulene for use as opto-electronic materials. Among the investigated compounds only **3-H**$^+$ and to a lesser extent **4-H**$^+$ showed a significant increase in emission intensity upon protonation. While **4-H**$^+$ displayed a slightly higher intensity, the emission wavelength of **3-H**$^+$ was found to be substantially more red-shifted. DFT calculations were carried out to explain the experimental observations. These results led to the conclusion that azulene incorporated as a core structure in optoelectronic materials exhibits very weak $S_0 \rightarrow S_2$ and corresponding $S_2 \rightarrow S_0$ transitions if both substitutions are situated at the five-membered ring. It is required that at least one substitution be present in the seven-membered ring in order to obtain fluorescence materials that display significant stimuli response behavior. Based on these findings, studies involving the incorporation of 2,6-connected azulene into macromolecules and subsequent evaluation of the stimuli responsive behavior as well as its potential in opto-electronic applications are currently under way.

Acknowledgements

This work was supported by the Swiss National Science Foundation NRP 62 Smart Materials Program (Grant no. 406240-126142). Support from the University of Zurich and Prof. Heinz Berke is gratefully acknowledged.

Notes and references

1 V. Kamm, G. Battagliarin, I. A. Howard, W. Pisula, A. Mavrinskiy, C. Li, K. Müllen and F. Laquai, *Adv. Energy Mater.*, 2011, **1**, 297–302.
2 R. Mauer, I. A. Howard and F. Laquai, *J. Phys. Chem. Lett.*, 2010, **1**, 3500–3505.
3 S. W. Thomas, G. D. Joly and T. M. Swager, *Chem. Rev.*, 2007, **107**, 1339–1386.
4 V. Coropceanu, J. Cornil, D. A. da Silva Filho, Y. Olivier, R. Silbey and J.-L. Brédas, *Chem. Rev.*, 2007, **107**, 926–952.
5 A. Heckmann and C. Lambert, *Angew. Chem., Int. Ed.*, 2012, **51**, 326–392.
6 M. A. Rahman, P. Kumar, D. S. Park and Y. B. Shim, *Sensors*, 2008, **8**, 118–141.
7 E. J. Feldmeier and C. Melzer, *Org. Electron.*, 2011, **12**, 1166–1169.
8 C. Zhu, L. Liu, Q. Yang, F. Lv and S. Wang, *Chem. Rev.*, 2012, **112**, 4687–4735.
9 I. A. Howard, R. Mauer, M. Meister and F. Laquai, *J. Am. Chem. Soc.*, 2010, **132**, 14866–14876.
10 A. P. de Silva, H. Q. N. Gunaratne, T. Gunnlaugsson, A. J. M. Huxley, C. P. McCoy, J. T. Rademacher and T. E. Rice, *Chem. Rev.*, 1997, **97**, 1515–1566.
11 S. Malashikhin and N. S. Finney, *J. Am. Chem. Soc.*, 2008, **130**, 12846–12847.
12 S. A. Malashikhin, K. K. Baldridge and N. S. Finney, *Org. Lett.*, 2010, **12**, 940–943.
13 A. P. de Silva and T. E. Rice, *Chem. Commun.*, 1999, 163–164.
14 B. Esser and T. M. Swager, *Angew. Chem., Int. Ed.*, 2010, **49**, 8872–8875.
15 J. Bouffard, Y. Kim, T. M. Swager, R. Weissleder and S. A. Hilderbrand, *Org. Lett.*, 2008, **10**, 37–40.
16 T. Gupta and M. E. van der Boom, *J. Am. Chem. Soc.*, 2006, **128**, 8400–8401.
17 T. Gupta, R. Cohen, G. Evmenenko, P. Dutta and M. E. van der Boom, *J. Phys. Chem. C*, 2007, **111**, 4655–4660.
18 N. J. Turro, *Modern Molecular Organic Photochemistry*, University Science Books, Sausalito, CA, 1991.
19 P. G. Lacroix, I. Malfant, G. Iftime, A. C. Razus, K. Nakatani and J. A. Delaire, *Chem.–Eur. J.*, 2000, **6**, 2599–2608.
20 D. R. Mitchell and G. D. Gillispie, *J. Phys. Chem.*, 1989, **93**, 4390–4393.
21 Y. Yamaguchi, Y. Maruya, H. Katagiri, K. Nakayama and Y. Ohba, *Org. Lett.*, 2012, **14**, 2316–2319.
22 K. Kurotobi, K. S. Kim, S. B. Noh, D. Kim and A. Osuka, *Angew. Chem., Int. Ed.*, 2006, **45**, 3944–3947.
23 P. Wang, P. Zhu, C. Ye, A. E. Asato and R. S. H. Liu, *J. Phys. Chem. A*, 1999, **103**, 7076–7082.

24 R. S. H. Liu, R. S. Muthyala, X.-s. Wang, A. E. Asato, P. Wang and C. Ye, *Org. Lett.*, 2000, **2**, 269–271.
25 E. Amir, R. J. Amir, L. M. Campos and C. J. Hawker, *J. Am. Chem. Soc.*, 2011, **133**, 10046–10049.
26 M. Koch, O. Blacque and K. Venkatesan, *Org. Lett.*, 2012, **14**, 1580–1583.
27 M. Murai, E. Amir, R. J. Amir and C. J. Hawker, *Chem. Sci.*, 2012, **3**, 2721–2725.
28 S. Dutta, S. Lakshmi and S. K. Pati, *Bull. Mater. Sci.*, 2008, **31**, 353–358.
29 J. R. Dias, *J. Phys. Org. Chem.*, 2007, **20**, 395–409.
30 H. Kim, N. Schulte, G. Zhou, K. Müllen and F. Laquai, *Adv. Mater.*, 2011, **23**, 894–897.
31 N. C. Thanh, M. Ikai, T. Kajioka, H. Fujikawa, Y. Taga, Y. Zhang, S. Ogawa, H. Shimada, Y. Miyahara, S. Kuroda and M. Oda, *Tetrahedron*, 2006, **62**, 11227–11239.
32 X.-Y. Chen, C. Barnes, J. R. Dias and T. C. Sandreczki, *Chem.–Eur. J.*, 2009, **15**, 2041–2044.
33 K. H. H. Fabian, A. H. M. Elwahy and K. Hafner, *Eur. J. Org. Chem.*, 2006, 791–802.
34 V. V. Filichev, M. C. Nielsen, N. Bomholt, C. H. Jessen and E. B. Pedersen, *Angew. Chem., Int. Ed.*, 2006, **45**, 5311–5315.
35 S. Ito, H. Inabe, T. Okujima, N. Morita, M. Watanabe and K. Imafuku, *Tetrahedron Lett.*, 2000, **41**, 8343–8347.
36 S. Ito, H. Inabe, T. Okujima, N. Morita, M. Watanabe, N. Harada and K. Imafuku, *J. Org. Chem.*, 2001, **66**, 7090–7101.
37 K. H. H. Fabian, A. H. M. Elwahy and K. Hafner, *Tetrahedron Lett.*, 2000, **41**, 2855–2858.
38 M. V. Barybin, M. H. Chisholm, N. S. Dalal, T. H. Holovics, N. J. Patmore, R. E. Robinson and D. J. Zipse, *J. Am. Chem. Soc.*, 2005, **127**, 15182–15190.
39 S. Ito, M. Ando, A. Nomura, N. Morita, C. Kabuto, H. Mukai, K. Ohta, J. Kawakami, A. Yoshizawa and A. Tajiri, *J. Org. Chem.*, 2005, **70**, 3939–3949.
40 T. R. Maher, A. D. Spaeth, B. M. Neal, C. L. Berrie, W. H. Thompson, V. W. Day and M. V. Barybin, *J. Am. Chem. Soc.*, 2010, **132**, 15924–15926.
41 K. Nakagawa, T. Yokoyama, K. Toyota, N. Morita, S. Ito, S. Tahata, M. Ueda, J. Kawakami, M. Yokoyama, Y. Kanai and K. Ohta, *Tetrahedron*, 2010, **66**, 8304–8312.
42 T. C. Holovics, R. E. Robinson, E. C. Weintrob, M. Toriyama, G. H. Lushington and M. V. Barybin, *J. Am. Chem. Soc.*, 2006, **128**, 2300–2309.
43 M. Kivala and F. o. Diederich, *Acc. Chem. Res.*, 2009, **42**, 235–248.
44 D. Balschukat and E. V. Dehmlow, *Chem. Ber.*, 1986, **119**, 2272–2288.
45 S. Carret, A. Blanc, Y. Coquerel, M. Berthod, A. E. Greene and J.-P. Deprés, *Angew. Chem., Int. Ed.*, 2005, **44**, 5130–5133.
46 See ESI.†
47 T. Nozoe, T. Asao and M. Oda, *Bull. Chem. Soc. Jpn.*, 1974, **47**, 681–686.
48 T. Nozoe, K. Takase and N. Shimazaki, *Bull. Chem. Soc. Jpn.*, 1964, **37**, 1644–1648.
49 R. Brettle, D. A. Dunmur, S. Estdale and C. M. Marson, *J. Mater. Chem.*, 1993, **3**, 327–331.
50 It has to be mentioned that for compound **1** higher concentrations of superacid were needed for full conversion into the protonated species **1**-H^+.
51 For **3** and **4** concentrations resulting in an O.D. of 0.1 a.u. in the UV-vis absorption spectra were chosen for the measurements of the UV-vis emission spectra. In the case of **1** and **2** concentrations resulting in an O.D. of 0.3 a.u. were chosen to determine the fluorescence properties.
52 M. J. Frisch, G. W. Trucks, H. B. Schlegel, G. E. Scuseria, M. A. Robb, J. R. Cheeseman, G. Scalmani, V. Barone, B. Mennucci, G. A. Petersson, H. Nakatsuji, M. Caricato, X. Li, H. P. Hratchian, A. F. Izmaylov, J. Bloino, G. Zheng, J. L. Sonnenberg, M. Hada, M. Ehara, K. Toyota, R. Fukuda, J. Hasegawa, M. Ishida, T. Nakajima, Y. Honda, O. Kitao, H. Nakai, T. Vreven, J. A. Montgomery, Jr, J. E. Peralta, F. Ogliaro, M. Bearpark, J. J. Heyd, E. Brothers, K. N. Kudin, V. N. Staroverov, T. Keith, R. Kobayashi, J. Normand, K. Raghavachari, A. Rendell, J. C. Burant, S. S. Iyengar, J. Tomasi, M. Cossi, N. Rega, J. M. Millam, M. Klene, J. E. Knox, J. B. Cross, V. Bakken, C. Adamo, J. Jaramillo, R. Gomperts, R. E. Stratmann, O. Yazyev, A. J. Austin, R. Cammi, C. Pomelli, J. W. Ochterski, R. L. Martin, K. Morokuma, V. G. Zakrzewski, G. A. Voth, P. Salvador, J. J. Dannenberg, S. Dapprich, A. D. Daniels, O. Farkas, J. B. Foresman, J. V. Ortiz, J. Cioslowski and D. J. Fox, *Gaussian 09, Revision B.01*, Gaussian, Inc., Wallingford CT, 2010.
53 C. Adamo and V. Barone, *J. Chem. Phys.*, 1999, **110**, 6158–6170.
54 J. T. H. Dunning, *J. Chem. Phys.*, 1989, **90**, 1007–1023.
55 R. E. Stratmann, G. E. Scuseria and M. J. Frisch, *J. Chem. Phys.*, 1998, **109**, 8218–8224.
56 R. Bauernschmitt and R. Ahlrichs, *Chem. Phys. Lett.*, 1996, **256**, 454–464.
57 M. E. Casida, C. Jamorski, K. C. Casida and D. R. Salahub, *J. Chem. Phys.*, 1998, **108**, 4439–4449.
58 V. Barone and M. Cossi, *J. Phys. Chem. A*, 1998, **102**, 1995–2001.
59 M. Cossi, N. Rega, G. Scalmani and V. Barone, *J. Comput. Chem.*, 2003, **24**, 669–681.